Citation: Cell Death and Disease (2011) 2, e210; doi:10.1038/cddis.2011.79

www.nature.com/cddis

Increased hippocampal CA1 density of serotonergic terminals in a triple transgenic mouse model of Alzheimer's disease: an ultrastructural study

HN Noristani[1], RS Meadows[1], M Olabarria[1], A Verkhratsky[1,2,3] and JJ Rodríguez*[,2,3,4,5]

Alzheimer's disease (AD) is a neurodegenerative pathology that deteriorates mnesic functions and associated brain regions including the hippocampus. Serotonin (5-HT) has an important role in cognition. We recently demonstrated an increase in 5-HT transporter (SERT) fibre density in the hippocampal CA1 in an AD triple transgenic mouse model (3xTg-AD). Here, we analyse the ultrastructural localisation, distribution and numerical density (N_v) of hippocampal SERT axons (SERT-Ax) and terminals (SERT-Te) and their relationship with SERT fibre sprouting and altered synaptic N_v in 3xTg-AD compared with non-transgenic control mice. 3xTg-AD animals showed a significant increase in SERT-Te N_v in CA1 at both, 3 (95%) and 18 months of age (144%), being restricted to the CA1 stratum moleculare (S. Mol; 227% at 3 and 180% at 18 months). 3xTg-AD animals also exhibit reduced N_v of perforated axospinous synapses (PS) in CA1 S. Mol (56% at 3 and 52% at 18 months). No changes were observed in the N_v of symmetric and asymmetrical synapses or SERT-Ax. Our results suggest that concomitant SERT-Te N_v increase and PS reduction in 3xTg-AD mice may act as a compensatory mechanism maintaining synaptic efficacy as a response to the AD cognitive impairment.

Cell Death and Disease (2011) **2,** e210; doi:10.1038/cddis.2011.79; published online 15 September 2011
Subject Category: Neuroscience

Alzheimer's disease (AD) is an age-related, irreversible and progressive neurodegenerative disease that deteriorates memory and cognition.[1] Neuropathological hallmarks of AD include neuritic plaques (amyloid beta (Aβ)), neuro-fibrillary tangles, neuronal death and synaptic loss, which occurs early in AD, and is linked to impaired synaptic connectivity and plasticity.[2,3]

Although, AD affects primarily the cholinergic system,[4] other neurotransmitter systems are also implicated such as glutamate[5] and serotonin (5-HT).[6,7] Majority of 5-HT neurones are located within the dorsal and median raphe nuclei projecting to numerous brain regions including the thalamus, amygdala, cortex and the hippocampus, where they have important role in mnesic and cognitive functions.[8,9] AD patients exhibit reduced 5-HT neurotransmission, which correlates with disease severity.[10] Treatment with selective serotonin re-uptake inhibitors (SSRIs) and specific 5-HT receptor ligands improves cognition in AD patients.[6]

The degree and importance of changes in the 5-HT system in AD remains elusive in human studies, however, experiments on animal models indicate its pathological relevance. $APP_{swe}/PS1_{\Delta E9}$ double transgenic mice display degeneration of 5-HT fibres, while $APP_{Sw,Ind}$ transgenic mice overexpressing APP Swiss/Indian mutations show stable 5-HT fibre density in parietal cortex and the hippocampus.[11,12] However, subsequent study in $APP_{swe}/PS1_{\Delta E9}$ transgenic mice revealed no alterations in 5-HT transporter binding sites (measured using [^{3}H]-escitalopram radioligand) up to 11 months of age despite Aβ accumulation in the cortex and the hippocampus.[13] Similarly, increased 5-HT fibre sprouting was reported following neurotoxin lesion and Aβ accumulation in striatum and hippocampus[14–17] (see also Table 1). In addition, other transgenic mice (APP-23) show aberrant non-5-HT hippocampal axonal sprouting, which is directly related to Aβ accumulation.[18] Serotonin transporter (SERT) is expressed in serotonergic axons and axonal terminals being critical for 5-HT re-uptake.[19] Recently, we reported increased hippocampal SERT-immunoreactive (SERT-IR) fibres density in the triple transgenic (3xTg-AD) mouse model of AD,[7] which mimics the spatiotemporal pathology and mnesic alterations of AD.[20] Interestingly, the increase in SERT-IR fibre density is more evident in proximity to amyloid plaques suggesting that aberrant SERT-IR axonal sprouting and amyloid deposition are closely linked in AD neuropathology.[7]

Studies of synaptic density in AD patients and transgenic mouse models of AD also reveal inconsistent results. Whereas post-mortem studies show a steady decrease in synapses,[21,22] different transgenic mouse models exhibit

[1]Faculty of Life Sciences, The University of Manchester, Manchester, UK; [2]Institute of Experimental Medicine, ASCR, Videnska 1083, 142 20, Prague, Czech Republic; [3]IKERBASQUE, Basque Foundation for Science, 48011 Bilbao, Spain; [4]Department of Neurosciences, University of the Basque Country UPV/EHU, 48940 Leioa, Spain and [5]Instituto de Investigación Sanitaria Biodonostia, Hospital Donostia, 20014 San Sebastián, Spain
*Corresponding author: JJ Rodríguez, IKERBASQUE, Department of Neuroscience, University of the Basque Country UPV/EHU, Technological Park, Building 205, Floor -1, Laida Bidea, 48170-Zamudio, Vizkaia, Spain. Tel: +34 946018305; Fax: +34 946018289; E-mail: j.rodriguez-arellano@ikerbasque.org
Keywords: Alzheimer's disease; serotonin; serotonin transporter; electron microscopy; hippocampus; plasticity
Abbreviations: 3xTg-AD, triple transgenic mouse model of Alzheimer's disease; 5-HT, serotonin; AD, Alzheimer's disease; Aβ, amyloid beta; N_v, numerical density; S. Mol, stratum lacunosum moleculare; S. Or, stratum oriens; S. Py, stratum pyramidale; S. Rad, stratum radiatum; SERT, serotonin transporter; SERT-Ax, serotonin transporter-positive axons; SERT-Te, serotonin transporter positive terminals; SSRI, selective serotonin re-uptake inhibitor
Received 16.5.11; revised 01.7.11; accepted 12.7.11; Edited by D Bano

Table 1 Summary of studies on 5-HT alterations in animal models of Alzheimer's disease

AD model	Neuropathology	Brain area investigated	5-HT alteration	Reference
$APP_{swe}/PS1_{\Delta E9}$	Plaques	C, Am, H	5-HT fibre degeneration (12 and 18 months)	Liu *et al.*[11]
APP_{Swe}	Plaques	H	Aberrant non-5-HT axonal sprouting (18–20 months)	Phinney *et al.*[18]
Intrahippocampal $A\beta_{(1-40)}$ injection	Aggregated amyloid material	H	Increased 5-HT activity within the vicinity of injection site	Verdurand *et al.*[16]
Intrastriatal ibotenic acid injection	Neurodegeneration	S	Vigorous sprouting of 5-HT fibres	Zhou *et al.*[17]
MBN NMDA injection	Increased APP expression+cholinergic lesion	MBN	Abundant sprouting of 5-HT fibres within damaged area	Harkany *et al.*[14]
MBN $A\beta_{(1-42)}$ injection	Cholinergic lesion	MBN	5-HT fibre sprouting	Harkany *et al.*[15]
$APP_{swe}/PS1_{\Delta E9}$	Plaques	FC, PreC, H	No change	Holm *et al.*[13]
$hAPP_{Sw,Ind}$	Plaques	H	No change	Aucoin *et al.*[12]
3xTg-AD	Plaques and tangles	H	Biphasic $>65\%$ increased SERT-Fibre density (3 and 18 months)	Noristani *et al.*[7]

Abbreviations: Am, Amygdala; APP, amyloid precursor protein; C, cortex; FC, frontal cortex; H, hippocampus; MBN, magnocellular nucleus basalis; NMDA, *N*-methyl-D-aspartate, PreC, prefrontal cortex; S, striatum

either increase, decrease or no overall alterations[23,24] (see also Supplementary Table 1). Indeed, 3xTg-AD mice show no changes in total synapse density[25] although the numerical density (N_v) of hippocampal perforated axospinous synapses seems to be reduced.[26]

We recently reported increased SERT-IR fibre density in the CA1 stratum lacunosum moleculare (S. Mol) of the hippocampus in 3xTg-AD mice.[7] This increase in SERT-IR fibre density initially appears at 3 months, which is in parallel with the evident intraneuronal accumulation of $A\beta$.[7,20] However, SERT-IR fibre density between 6, 9 and 12 months of age, is comparable to non-transgenic (non-Tg), while there is a late sprouting recurrence at 18 months, concomitant with the build-up of large extracellular neuritic plaques in 3xTg-AD animals.[7,20] In this study, we extend our previous findings by analysing the ultrastructural changes in hippocampal SERT axons (SERT-Ax), terminals (SERT-Te) and their association with synaptic N_v and connectivity in the hippocampus in 3xTg-AD compared with non-Tg control, by using a quantitative three-dimensional immunoperoxidase method, at these two ostensibly key points in either the start-up of anomalous intraneuronal $A\beta$ accumulation (3 months) and the consolidation of $A\beta$ neuropil plaque formation and aggregation (18 months).

Results

At light microscopic level, in both 3xTg-AD and non-Tg control animals SERT-immuoreactive (SERT-IR) fibres were heterogeneously distributed throughout the hippocampal formation (Figures 1, 2a and b). SERT-IR fibres appeared mainly as fine and thick processes with numerous varicosities, which are characteristic of axonal profiles (Figures 1c, d, 2a and b). The highest densities of SERT-IR fibres are evident in the S. Mol of CA1 area (Figures 1c, d, 2a and b). Strata radiatum and oriens exhibited moderate expression while the lowest densities of SERT-IR fibres are present in the stratum pyramidale (S. Py). The 3xTg-AD group showed increased density of SERT-IR fibres in the S. Mol of CA1 exclusively at 3 and 18 months compared with age-matched controls (Figures 1c, d, 2a and b), as shown by augmented SERT-IR fibre optical and N_v, which corresponded to our previous and recently described findings during the progression of AD.[7] Increased SERT-IR fibre density, in 3xTg-AD, was even more evident in the proximity of $A\beta$ plaques (Figures 2d–f).

Ultrastructural distribution of hippocampal SERT profiles. SERT-EM analysis confirmed that the majority of SERT-IR profiles were small axons and axon terminals and/or varicosities with different size and morphological features according to their raphe nuclei origin (Figures 3a, b, d–f and 4c–f).[7] SERT-IR profiles were identified by the presence of amorphous electron-dense DAB reaction product that was mainly associated with the plasma membrane of axons and terminals (Figures 3d–f and 4c–f) with or without association with the synaptic specialisation (Figure 3a and d–f). From the 17 993 axonal profiles analysed, 592 (3.3%) contained peroxidase labelling for SERT. The majority of SERT-IR profiles consisted of morphologically heterogeneous population of axonal terminals and/or varicosities (SERT-Te) that made up 81% of the SERT contained profiles ($n=479$ out of 592; Figures 3a, b, d–f, 4c–f, 5b–e). Occasionally, the labelling was directly associated with cytoplasmic organelles, including dense core vesicles, which are characteristic of serotonergic terminals (Figure 3f).[19] Dense labelling for SERT was also observed in small unmyelinated axons (SERT-Ax), which were predominantly apposed to other small axons and/or terminals (Figure 3c). SERT-Ax comprised 17% of the SERT-IR profiles ($n=104$ out of 592) and was seldomly in contact with dendritic profiles. SERT labelling was absent in postsynaptic sites and was rarely observed in glial profiles. From the 479 immuno-labelled SERT-Te identified in this study, only 64 (13%) showed synaptic specialisation mostly represented by asymmetrical synapses with dendritic spines and dendrites (Figures 3a and b). SERT-Te area varied in size from 0.12 to 1.01 μm^2 (mean 0.2 ± 0.01 μm^2). The main postsynaptic target of SERT-Te terminals were unlabelled dendrites onto which these terminals establish asymmetrical

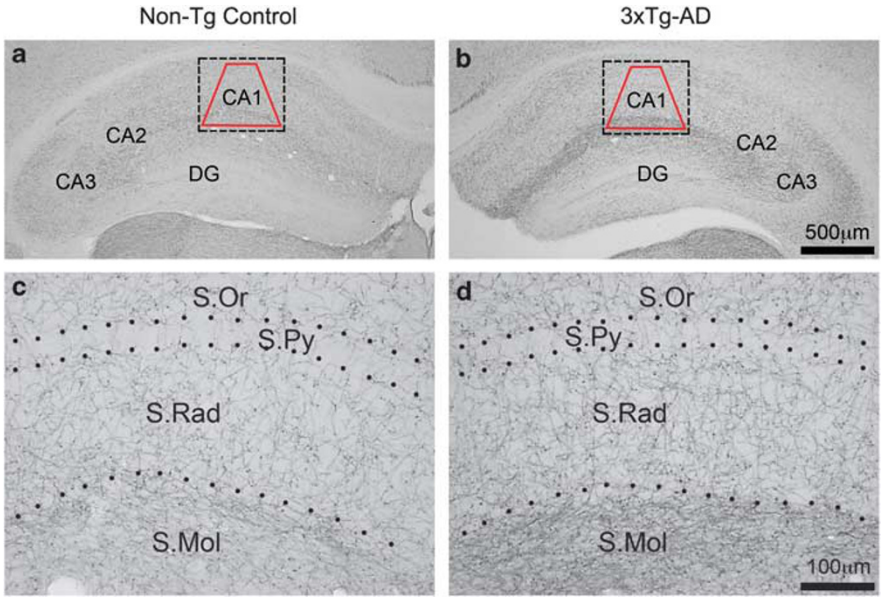

Figure 1 Brightfield micrographs illustrating the distribution of SERT-IR fibres in the dorsal hippocampus of 3 months old non-Tg control (**a**) and 3xTg-AD mice (**b**) and the respective high magnification details of the CA1 subfield area of the hippocampus that was selected for the electron microscopic analysis (**c** and **d**). Hippocampal sections were selected at identical anatomical levels between the different animals to ensure an exact and equivalent sampling. Scale bar 500 μm (**a** and **b**), 100 μm (**c** and **d**). DG, dentate gyrus

synapses, which sometimes localised in a close vicinity to glutamatergic excitatory synapses (Figures 3a, 4c–f, 5b–e).

Temporal changes in SERT-Te N_v and size in 3xTg-AD mice. We observed an increase in SERT-Te N_v in the CA1 subfield of the hippocampus in a strata-specific manner (Figures 4a and b). The global analysis showed a significant increase in SERT-Te N_v at 3 and 18 months in 3xTg-AD compared with control group (95%, $P=0.0436$ and 148%, $P=0.0064$, respectively; Figure 4a). A more detailed quantitative analysis of CA1 individual strata revealed that the increased SERT-Te N_v was restricted to the CA1 S. Mol, which also exhibited the highest density of SERT-IR fibres within the hippocampal formation in basal conditions (Figures 1c, d, 2a and b). This increase also appeared at the same ages doubling or almost doubling the values from age-matched control mice (227%, $P=0.0148$ at 3 months, and 180%, $P=0.0329$ at 18 months; Figure 4b). SERT-Te N_v showed no alterations in either stratum oriens (S. Or) or stratum radiatum (S. Rad) at any examined age ($P=0.5659$, $P=0.1948$ for S. Or and $P=0.0571$, $P=0.2607$ for S. Rad at 3 and 18 months, respectively; data not shown). The increase in SERT-Te N_v is associated with a generalised increase in their size as measured by determining their area, which was age specific (by 108%, $P=0.0264$ at 3 months and by 89%, $P=0.0474$, at 18 months; Figures 5a–e) but not strata specific. No age-associated changes were observed in either SERT-Te N_v or their size in 3xTg-AD animals between 3 and 18 months of age. However, non-Tg animals showed an age-associated decrease in SERT-Te N_v in the CA1 of the hippocampus (39% decrease, $P=0.0413$) although their size remain stable (Figures 4a and 5a). In addition, SERT-Ax N_v and size remained stable in 3x-Tg-AD and non-Tg control in all strata and examined ages.

Reduced N_v of perforated synapses in the hippocampus of 3xTg-AD mice. Synaptic elements and postsynaptic densities were heterogeneously distributed throughout the different hippocampal layers (Figures 3b, e, 4c–f, 5b–e) as revealed by the use of serial EM sections, which allowed us to distinguish and quantify different synapse populations, according to their postsynaptic densities and synaptic vesicles composition (see Supplementary Figure S1). Symmetric synapses have thin pre- and postsynaptic densities with axons containing pleomorphic (round and elongated) synaptic vesicles (Supplementary Figure S1A), while asymmetric synapses displayed round synaptic vesicles in the axons and were characterised by the presence of a thin presynaptic density and with a thick and more prominent postsynaptic membrane specialisation[27] (Supplementary Figure S1B). Some of these asymmetric synapses presented a notable discontinuity (>50 nm) in the electron density of the postsynaptic junction as previously described[27] being considered as perforated (Supplementary Figure S1C). The majority of the total unlabelled ($SERT^-$) identified synapses were asymmetric being characterised by a thin pre- and a thick postsynaptic membrane specialisation (Figures 3e and e). In total, 11 108 $SERT^-$ synapses were identified of which 10 889 (98.03%) were asymmetrical type between axons and dendritic spines; the remaining 219 (2%) were symmetrical synapses mainly established onto dendrites and dendritic shafts (Figure 3a). Only 7.9% (863) of the asymmetric synapses were identified as perforated.

Although, global analysis of hippocampal CA1 area showed no difference in N_v of total, symmetric and asymmetric $SERT^-$

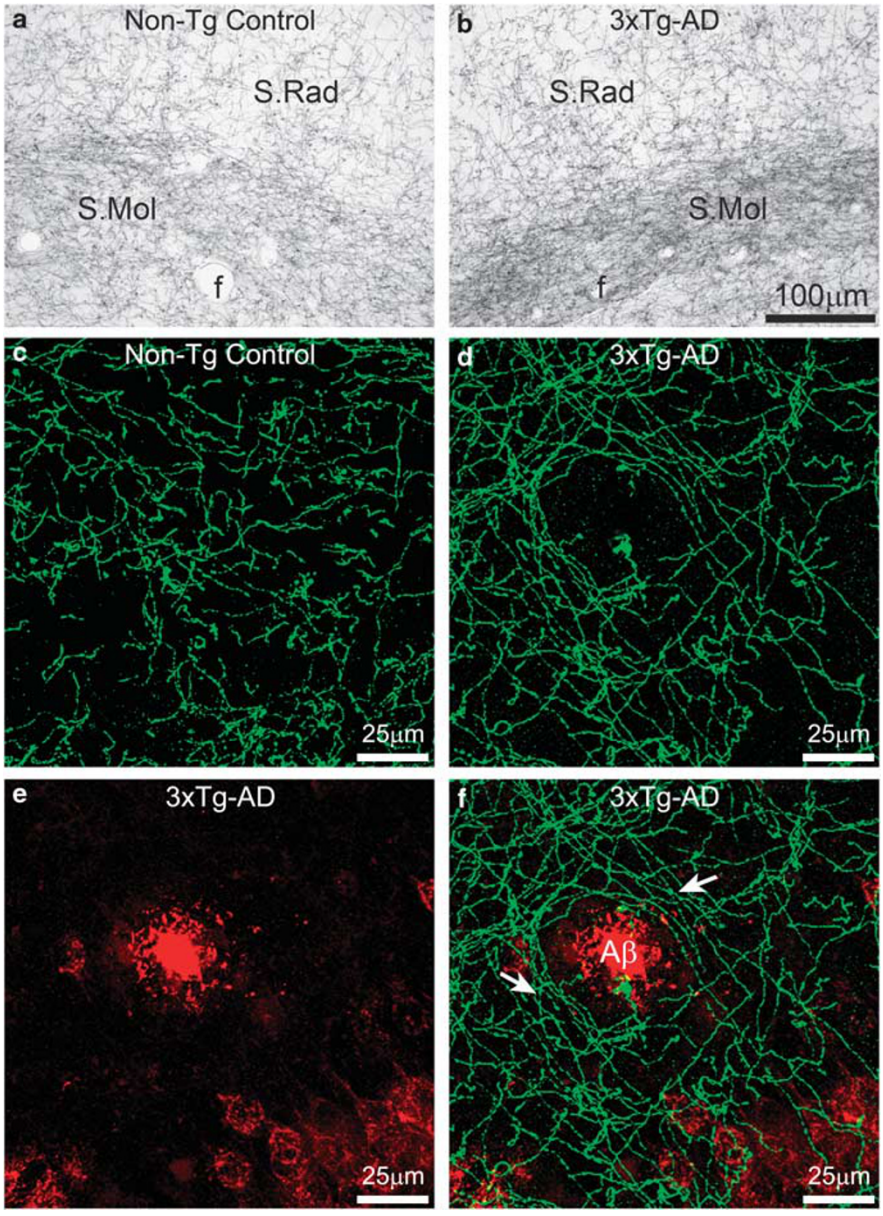

Figure 2 Brightfield micrographs showing SERT-IR fibres in the dorsal hippocampus of 18 months old non-Tg control (**a**) and 3xTg-AD mice (**b**). Dual confocal micrographs showing SERT-IR fibres in the dorsal hippocampus of 18 months old non-Tg control (**c**), and a 3xTg-AD (**d**), the latter containing Aβ plaques (**e**) showing SERT-IR fibres specific sprouting adjacent to Aβ plaques within the CA1 subfield of the hippocampus in a 18 month 3xTg-AD animal (**f**, merged image). Scale bar 100 μm (**a** and **b**), 25 μm **c, d, e** and **f**. f, hippocampal fissure

synapses; there was a significant decrease in perforated axospinous N_v in 3xTg-AD compared with non-Tg control (Figure 6c). Analysis of the whole hippocampus revealed significant decrease in perforated axospinous N_v in 3xTg-AD animals at 3 but not at 18 months of age (64% loss, $P=0.0056$ and 39% loss, $P=0.1453$). The layer-specific analysis also revealed that the S. Mol exhibits significant deficit in N_v of perforated axospinous synapses (Figure 7c) at 3 and 18 months compared with age-matched control (56% loss, $P=0.0260$ and 50% loss, $P=0.0394$). Furthermore, the non-Tg control group also showed an age-associated decrease in perforated axospinous N_v both in CA1 subfield of the hippocampus and S. Mol of the CA1 (38% loss, $P=0.0260$ and 34% loss, $P=0.0070$, Figures 6c and 7c), this was not the case for N_v of other types of $SERT^-$ synapses. However, we did not find any changes in the synaptic N_v specifically established by SERT-labelled ($SERT^+$) profiles when comparing 3xTg-AD with non-Tg animals either in the whole CA1 subfield or S. Mol ($P=0.4796$, $P=0.3739$ at 3 months and $P=0.1529$, $P=0.5185$ at 18 months, respectively (Figures 6d and 7d). $SERT^+$ synapses were mainly asymmetric synapses with dendritic spines and dendrites.

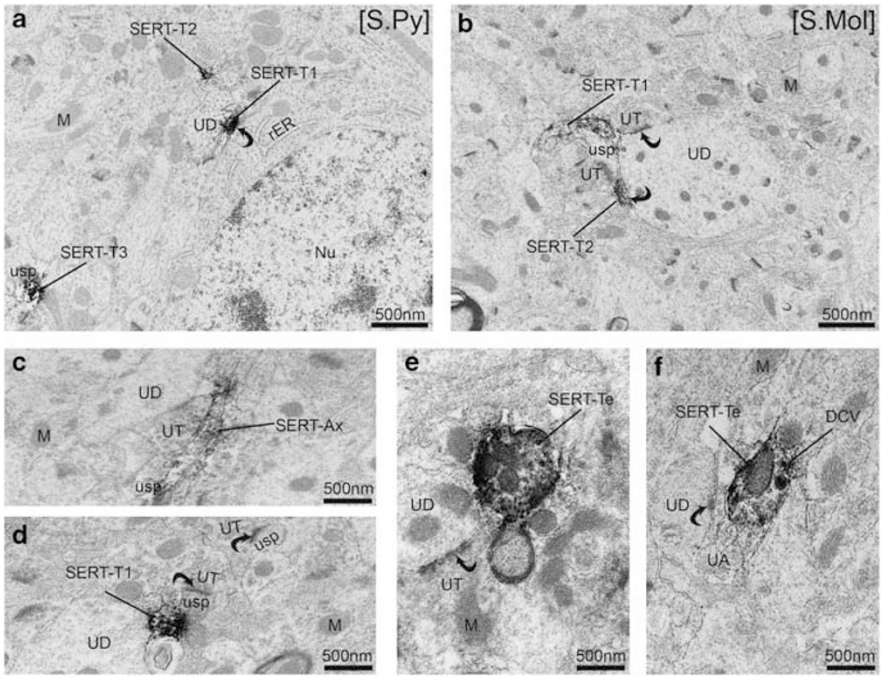

Figure 3 Electron micrographs showing morphological features of SERT axon terminals (SERT-Te) and SERT small axons (SERT-Ax) in the hippocampal CA1 subfield of 18 months old 3xTg-AD (**a** and **b**), 3 months old non-Tg control (**c** and **e**) and 18 months old non-Tg control (**d** and **f**). A: Peroxidase labelling for SERT-Te is seen within multiple terminals (T1-3) in the pyramidal cell layer of the hippocampus. One of them (SERT-T1) is forming an asymmetrical synapse (curved arrow) with an unlabelled dendrite (UD). (**b**) Immunoperoxidase labelling of two SERT-Te (T1-2) in the CA1 S. Mol, establishing two asymmetrical synaptic contacts (curved arrows) with an unlabelled dendrite (UD). (**c**) SERT plasmalemmal labelling in a small unmyelinated axon (SERT-Ax) in the CA1 S. Mol, which is apposed to an unlabelled terminal (UT) and an unlabelled dendritic spine (usp). (**d–f**) SERT immunoreactivity in small (**d**) and large axon terminals (**e** and **f**) in the CA1 S. Mol, showing in some cases the characteristic dense core vesicles (DCVs) of serotonergic terminals (**f**) and forming asymmetric synapses (curved arrows). Scale bar 500 nm (**a–f**). M, mitochondria; rER, rough endoplasmic reticulum; Nu, nucleus; UD, unlabelled dendrites; usp, unlabelled spine; UT, unlabelled axon terminal; UA, unlabelled axon

Ultrastructural analysis of $SERT^+$ synaptic specialisation also showed no difference in $SERT^+$ axo-spine and axo-dendritic synapses between 3xTg-AD and non-Tg control animals.

Discussion

Age-dependent and CA1 strata-specific increase in SERT terminals. Our main finding is that 3xTg-AD mice display an age-dependent increase in N_v of SERT-IR terminals. Global quantitative analysis of hippocampal CA1 revealed that SERT-Te N_v is increased at 3 and 18 months when compared with age-matched non-Tg controls. The increase in SERT-Te N_v is more evident within the S. Mol of CA1 area, which in normal conditions is also known to host the highest density of serotonergic projections in the hippocampal formation.[8] In addition, to the increased N_v the size of SERT-Te was also increased in the CA1 subfield of the hippocampus. No changes were observed in SERT-Ax N_v. These data suggest that there is an age-dependent increase in hippocampal serotonergic input that is closely associated with development of AD pathology in 3xTg-AD. Furthermore, our finding of increased SERT-Te N_v confirm our previous hypothesis of SERT fibres sprouting in the CA1 S. Mol of the hippocampus (as shown by increased optical and N_v of SERT-IR fibres) at 3 and 18 months 3xTg-AD mice compared with age-matched non-Tg control animals.[7] Serotonergic fibre sprouting is generally defined as fibre outgrowth reflected by increase in size and diameter of axons, appearance of new spindle varicosities with no sign of damaged SERT axons.[7,14,17] Serotonergic fibre sprouting may act as a compensatory mechanism by maintaining an overall stable hippocampal circuitry and synaptic connectivity. Thus, our results provide the first ultrastructural evidence for increased serotonergic input within the hippocampus of 3xTg-AD mouse model. Previously, increased 5-HT fibre sprouting was found only after acute brain damage such as Aβ, ibotenic acid and NMDA injections in rats (Table 1).[14–17] Similar changes in non-5-HT fibre sprouting were observed in the entorhinal cortex and thalamic nucleus in the APP23 transgenic mice.[18]

In 3xTg-AD mice, intracellular Aβ accumulation starts at an early age (3 months) that may also cause early damage to the affected neurones.[28] Extracellular deposition of $A\beta_{1-42}$ contributes to plaque formation, which in 3xTg-AD begins between 9 and 12 months of age and consolidates at 18 months, primarily targeting the CA1 hippocampal subfield and in particular stratum moleculare.[7,20] The 3xTg-AD mice exhibit age-related increase in extracellular build-up of plaques that continues into advanced age.[20] Indeed, previous studies including our recent studies in the same cohort of animals confirmed that the 3xTg-AD animals exhibit extensive Aβ and tau pathology at 18 months of age[7,20] (see also Figure 2e). Such massive build-up and consolidation of

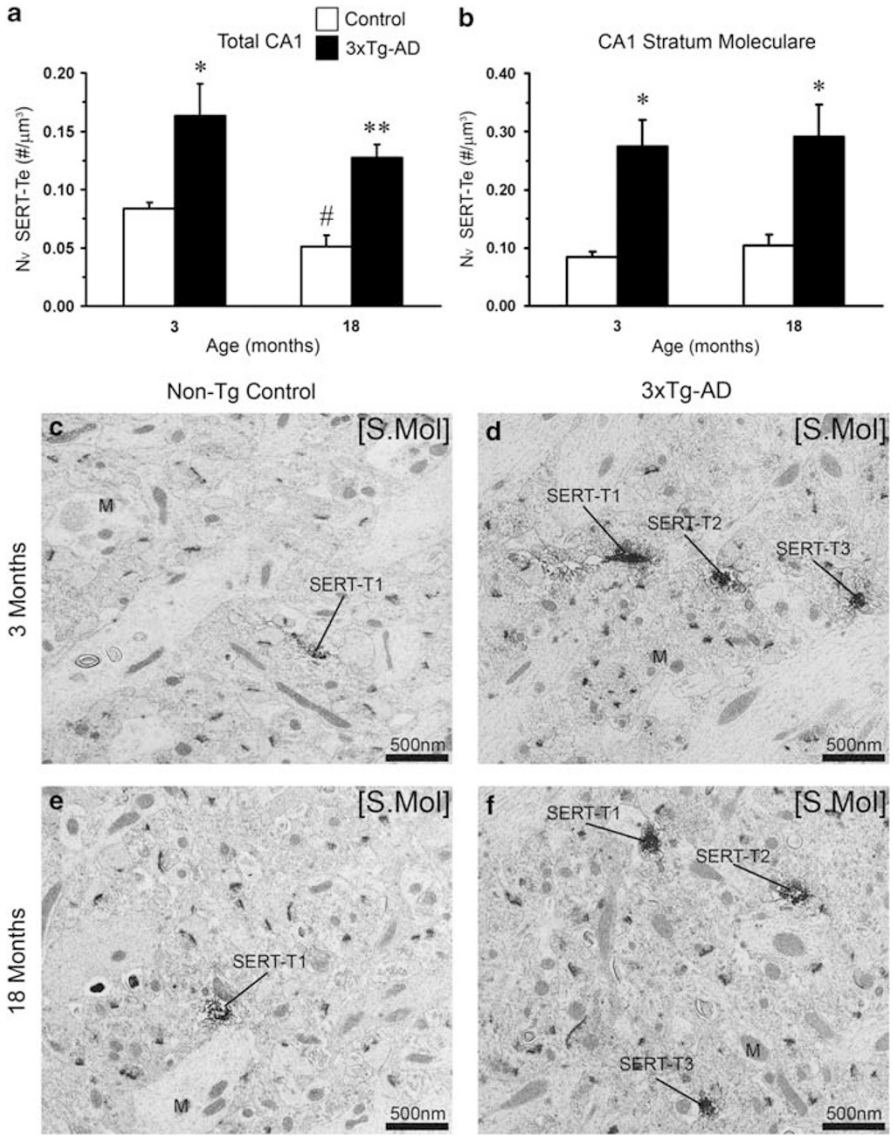

Figure 4 Bar graphs showing the age effect on SERT-Te N_v within overall CA1 subfield of the hippocampus (**a**) and stratum moleculare of the CA1 (**b**) at 3 and 18 months in non-Tg control and 3xTg-AD. Bars represent mean ± S.E.M. $^{*}P<0.05$, $^{**}P<0.01$ compared with age-matched non-Tg control, $^{\#}P<0.05$ compared with 3 months non-Tg control. (**c–f**) Representative electron micrographs illustrating SERT-Te density in the CA1 stratum moleculare subfield of the hippocampus at 3 and 18 months in non-Tg control (**c** and **e**) and 3xTg-AD mice (**d** and **f**). Scale bar 500 nm (**c–f**). M, mitochondria

plaques at a later age (18 months) may induce neurotoxic effects resulting in neuronal damage that in turn may also stimulate an increase in SERT-Te in 3xTg-AD.[7] Lack of SERT fibre sprouting at earlier ages (6 to 12 months) in 3xTg-AD animals may be due to lower level of extracellular amyloid accumulation in CA1 of the hippocampus, as well as to a less compromised synaptic connectivity compared with 18 months.[7] In agreement with this phenomenon, a recent study in the Aβ $APP_{swe}/PS1_{\Delta E9}$ double transgenic model with associated severe amyloid pathology showed no alteration in cortical and hippocampal SERT density up to 11 months of age.[13] In addition, our preliminary results suggest that SERT-IR fibre sprouting is further increased in the hippocampus at 24 months of age in 3xTg-AD animals, concomitant with formation of large extracellular Aβ plaques (Noristani *et al.,*[7] unpublished observation). Furthermore, our finding of early increase in SERT-Te (3 months) may indicate that this process could even start with the accumulation of intracellular $A\beta_{1-42}$,[20] which in turn might account for an initial protective response to restore hippocampal functionality.[7]

The neurotoxic effect of Aβ involves increased activation of glutamatergic neurotransmission and impairment of calcium homeostasis.[29] Increased 5-HT input may help to counteract neurotoxicity by inhibiting calcium influx and inducing membrane hyperpolarisation.[14,15] This effect is mediated by activation of $5\text{-}HT_{1A}$ and $5\text{-}HT_{1B}$ receptors that are highly expressed in the hippocampal formation.[30,31] In support of the above hypothesis, a recent study by Verdurand *et al.*[16] reported enhanced 5-HT neurotransmission and $5\text{-}HT_{1A}$ receptors expression following intrahippocampal infusion of

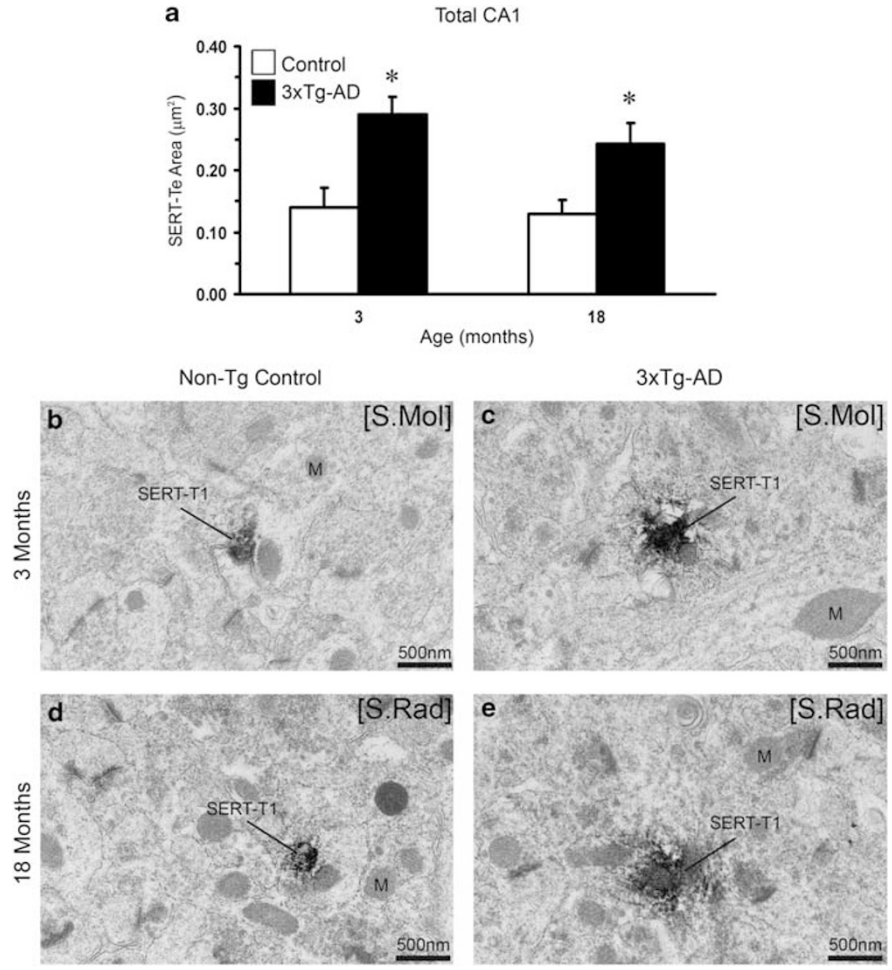

Figure 5 Bar graphs showing the age effect on SERT-Te area in the CA1 subfield of the hippocampus (**a**) at 3 and 18 months in non-Tg control and 3xTg-AD animals. Bars represent mean ± S.E.M. $^*P<0.05$. (**b–e**) Representative electron micrographs of the SERT-Te area in the CA1 subfield of the hippocampus in 3xTg-AD animals (**c** and **e**) compared with non-Tg control mice (**b** and **d**). Scale bar 500 nm (**b–e**). M, mitochondria

Aβ. Increased expression of hippocampal 5-HT_{1A} receptors was also reported in patients with mild cognitive impairment who exhibit greater risk of developing AD.[32] Therefore, an increased 5-HT input may represent an intrinsic protective mechanism in response to Aβ-induced excitotoxic damage.[7] In fact, increased SERT-Te area in 3xTg-AD suggests that these terminals might release greater quantities of neurotransmitter, thus enhancing the synaptic strength.

We have also observed a pronounced increase in SERT-Te N_v in the S. Mol. Such layer-specific effect may be due to the highest density of 5-HT projections compared with other hippocampal layers.[8] In addition, and as mentioned earlier, in 3xTg-AD animals excess extracellular Aβ plaques are evident in the S. Mol.[7] This combined phenomenon would account not only for the SERT-IR fibres sprouting but also directly affect the synaptic density and connectivity in the hippocampus.

AD-associated changes in synaptic density. Contrary to the accepted phenomenon linking AD to synaptic loss, we found no overall deficit in synaptic N_v in the hippocampal CA1 subfield.[3,22] Our results are in agreement with previous studies, which, by employing qualitative or semi quantitative light immunohistochemistry, reported no overall changes in synaptic-associated proteins such as synaptophysin in the hippocampus and in the cortex of APP23, PDAPP, PSAPP, APP_{Sw} and recently in 3xTg-AD animals (see Supplementary Table 1). Similarly, no changes in total N_v of synapses were observed in the pyramidal layer of the hippocampal CA1 in 3xTg-AD animals at 13 months of age.[26] We further extend this finding by analysing all the strata in 3xTg-AD animals up to 18 months of age. Although we found no changes in the overall synaptic N_v, there was a decrease in the N_v of perforated axospinous synapses in the CA1 area of the hippocampus and more specifically in the S. Mol that was evident at early age (3 months, 56%) and continued into advanced age (18 months, 52%). Our analysis has also shown that this synaptic population is affected during aging. The age-related decrease is consistent with previous results in aged rats in which hippocampal perforated synapses showed decrease in N_v and a reduction in the size of postsynaptic density[33,34] although others have reported no changes in total number of all perforated and non-perforated axospinous synapses.[35] One factor that may account for this discrepancy includes variations in hippocampal volume.[35]

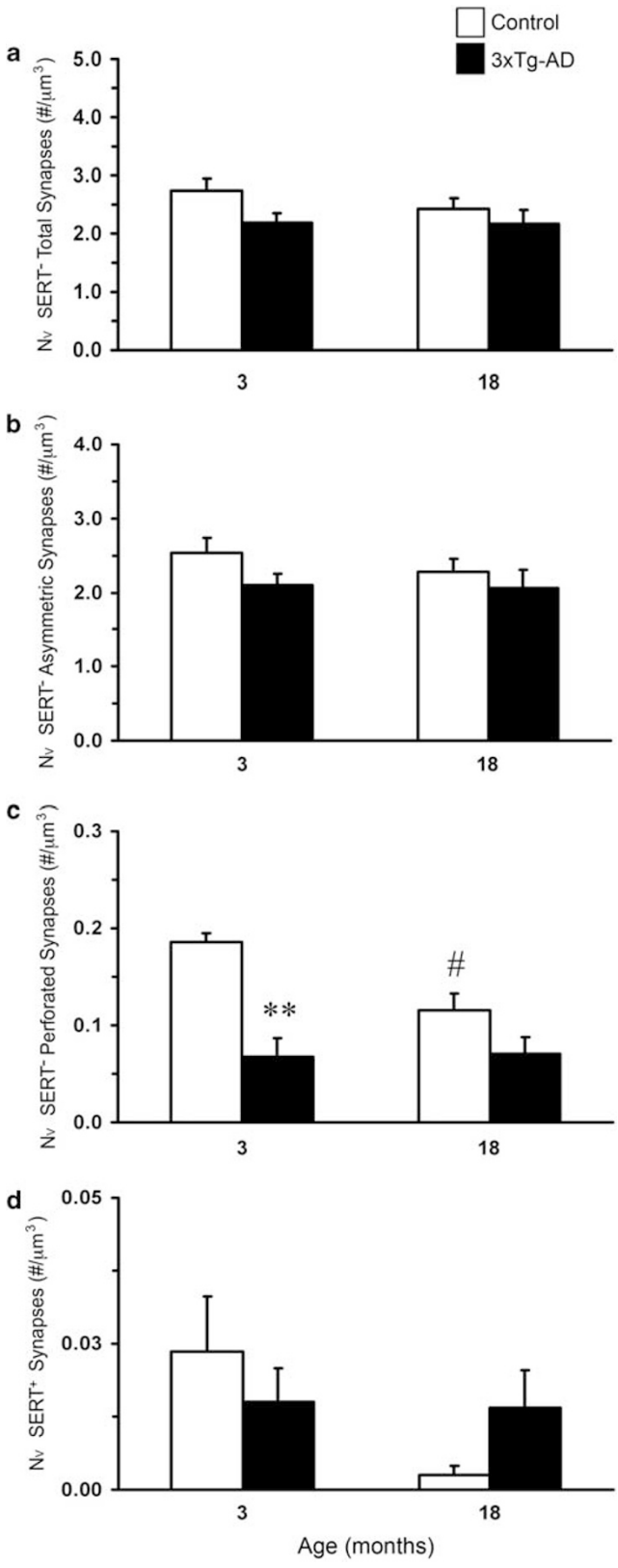

Figure 6 Bar graphs showing the age effect on unlabelled (SERT$^-$) total (**a**), asymmetrical (**b**), and perforated synapses (**c**) as well as the specific synaptic N_v of SERT-labelled (SERT$^+$) profiles (**d**) in the CA1 of the hippocampus at 3 and 18 months in non-Tg control and 3xTg-AD group. Bars represent mean ± S.E.M. $^{**}P<0.01$, $^{\#}P<0.05$

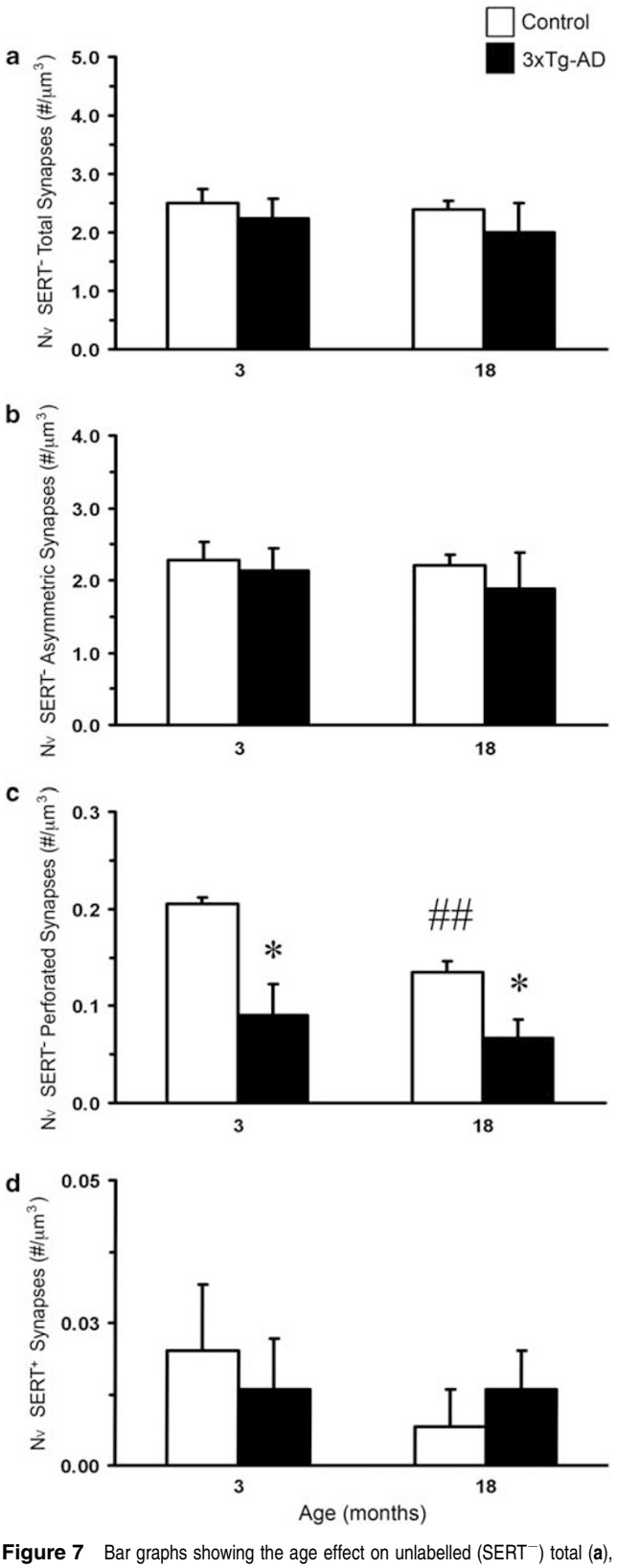

Figure 7 Bar graphs showing the age effect on unlabelled (SERT$^-$) total (**a**), asymmetrical (**b**), and perforated synapses (**c**) as well as the specific synaptic N_v of SERT-labelled (SERT$^+$) profiles (**d**) at 3 and 18 months in non-Tg control and 3xTg-AD in the CA1 S. Mol of the hippocampus. Bars represent mean ± S.E.M. ($n=3$). $^{*}P<0.05$, $^{\#\#}P<0.01$

Conflicting results have been reported in relation to hippocampal volume alterations in different transgenic models of AD.[36–40] Previous studies in single and double transgenic mouse models of AD including (PS1, APP/PS-1 and PSAPP mice) showed no alterations in hippocampal volume using longitudinal *in vivo* MRI scanning[36] or Cavalieri's principle for estimation of total hippocampal volume.[37,38] Contrary, Oberg *et al*.[39] reported decreased hippocampal volume in APP/PS1 double transgenic mice using *in vivo* longitudinal MRI scanning. On the other hand, Maheswaran *et al*.[40] have demonstrated increased hippocampal volume in the TASTPM mice showing severe amyloidosis, which could be associated with an accumulation of amyloid plaques and reactive glial cells. In this study, we analysed an equal hippocampal volume between 3xTg-AD and non-Tg control animals, which reliably eradicates the effect of possible volume alterations on synaptic N_v.[35,41] In addition, ultrathin section series were cut at a constant thickness (see Materials and methods section) between the two groups to avoid the bearing effect of section thickness on synaptic N_v.[41] Furthermore, the criteria we used for synapse determination includes not only the presence of postsynaptic density but also the occurrence of the adjacent presynaptic element containing the synaptic vesicles, which provides a reliable and un-biased estimation of synaptic N_v compared with that of just profile count.[41] Finally, and in parallel with the report in the majority of AD transgenic models, our findings are consistent with a recent electron microscopic study that also reported reduced N_v of perforated synapses in 3xTg-AD, when quantifying synapses per unit volume.[26]

Perforated axospinous synapses in the hippocampus have an important role in spatial and working memory.[33,34] Increased perforated synapses have been linked with the induction of long-term potentiation and enhanced memory performance in rodents.[42] Reduced perforated synapses show good correlation with deterioration of cognitive function including learning and memory.[33,34] Given the pivotal role of perforated axosinous synapses in cognitive function, the reduced N_v of perforated synapses that we have found may reflect the impaired synaptic plasticity and subsequent deterioration of learning and memory in 3xTg-AD animals.[20,26] In this direction, post-mortem studies on human tissue have consistently reported a decrease in synaptic density in the cortex and in the hippocampus.[21,22] In transgenic models, which exhibit plaque pathology, both an increase and a decrease in synaptic density was found in the neocortex and in the hippocampus.[23,24] Transgenic models with tangle pathology have also showed reduced hippocampal synaptic density[43] (see also Supplementary Table 1). Different factors may account for these controversies including differences in (i) transgenic models (ii) strains, (iii) age, (iv) brain area studied and (v) methods used to quantify synaptic density.[41]

In conclusion, this study suggest that sprouting of serotonergic axons is directly related with an increased N_v and area of SERT-Te that may act as a compensatory mechanism in maintaining overall synaptic efficacy. In addition, this increased serotonergic input may be an intrinsic neuroprotective response to counteract Aβ-induced neurotoxicity and altered hippocampal glutamatergic circuitry, as revealed by the decrease in asymmetric perforated N_v, accounting for the early behavioural alterations and later establishment of severe and permanent cognitive and mnesic impairments in AD. In fact, enhanced 5-HT neurotransmission via chronic treatment with SSRI (paroxetine) improves memory performance and retards the development of amyloid and tau pathologies in 3xTgAD mice.[44] Thus, increasing 5-HT neurotransmission in AD may provide a better therapeutic approach not only to improve behavioural abnormalities, but also to interfere with underlying neuropathology associated with AD.

Materials and Methods

All animal procedures were carried out in accordance with the United Kingdom Animals (Scientific Procedures) Act of 1986 under the license from the Home Office. All efforts were made to reduce the number of animals by following the 3Rs.

Animals. The procedures for generating 3xTg-AD mice have been described previously.[7,20] In brief, human APP cDNA harbouring the Swedish mutation (KM670/671NL) and human four repeat Tau, harbouring the P301L mutations were co-microinjected into single-cell embryos of homozygous PS1M146V knockin mice. The background of the PS1 knockin mice is a hybrid 129/C57BL6. The non-Tg control mice used were also from the same strain and genetic background as the PS1 knockin mice, but they harbour the endogenous wild-type mouse PS1 gene. All 3xTg-AD and non-Tg mice were obtained by crossing homozygous breeders. The animals were housed in the same-sex cage, kept in 12-h light–dark cycles with free access to food and water.

Fixation and tissue processing. Male 3xTg-AD and their respective non-Tg controls were anaesthetised with intraperitoneal injection of sodium pentobarbital (50 mg/kg) at 3 and 18 months of age ($n = 3$). Mice were perfused through the aortic arch with 3.75% acrolien (TAAB, Berkshire, UK) in a solution of 2% paraformaldehyde (Sigma, Gillingham, UK) and 0.1 M phosphate buffer (PB) pH 7.4, followed by 2% paraformaldehyde. Brains were then removed and cut into 4–5 mm coronal slabs of tissue consisting of the entire rostrocaudal extent of the hippocampus, as described previously.[7] The brain sections were post-fixed in 2% paraformaldehyde for 24 h and kept in 0.1 M PB, pH 7.4. Coronal sections of the brain were cut into 40–50 μM thickness using a vibrating microtome (VT1000S, Leica, Milton Keynes, UK). Free floating brain sections in 0.1 M PB, pH 7.4 were collected and stored in cryoprotectant solution containing 25% sucrose and 3.5% glycerol in 0.05 M PB at pH 7.4. Coronal vibratome hemisections at level -2.06 mm posterior to Bregma (dorsal hippocampus), were selected for immunohistochemistry according to the mouse brain atlas of Paxinos and Franklin.[45] To optimise the penetration of immunoreagents, the tissue sections were freeze-thawed as described previously.[27] For this procedure, the sections were (i) incubated in cryoprotectant solution containing 25% sucrose and 3.5% glycerol in 0.05 M PB, pH 7.4, (ii) rapidly immersed in chlorodifluoromethane, followed by liquid nitrogen and (iii) placed in 0.1 M PB at room temperature to thaw the tissue. Then the sections were rinsed in 0.1 M PB, followed by 0.1 M Trizma base saline (TS), pH 7.6.

Antibodies. A polyclonal rabbit antibody raised against a synthetic peptide sequence corresponding to amino acids 602–622 of rat 5HT transporter (Immunostar, Hudson, WI, USA) was used for determination of SERT-positive axons and terminals in the hippocampus. For the identification of Aβ plaques, we used a monoclonal mouse antiserum monoclonal antibody against amino acid resides 1–16 of beta amyloid (Covance, Emeryville, CA, USA). The specificity of the antibody has been reported previously using immunohistochemistry[7] and western blots.[46] To further determine the specificity of the antibody, adsorption controls were done using SERT peptide, which resulted in total absence of target labelling. Furthermore, omission of primary and/or secondary antibody also showed no immunoreactivity (data not shown).

Immunohistochemistry. The sections were incubated for 30 min in 30% methanol in 0.1 M PB and 3% hydrogenperoxide (H_2O_2; Sigma). Sections were then rinsed with 0.1 M PB for 5 min and placed in 1% sodium borohydride (Aldrich, Gilligham, UK) for 30 min. The sections were then washed with PB profusely before

rinsing in 0.1 M TS for 10 min. Brain sections were then incubated in 0.5% albumin bovine serum BSA (Sigma) in 0.1 M TS and 0.25% Triton (Sigma, × 100) for 30 min. Sections were incubated for 48 h at room temperature in primary antibody (rabbit anti-SERT, 1 : 2500, Immunostar). The sections were rinsed in 0.1 M TS for 30 min and incubated in 1 : 400 dilutions of biotinylated donkey anti-rabbit IgG (Jackson Immunoresearch, Stratech Scientific Ltd, Soham, UK) for 1 h at room temperature. Sections were rinsed with 0.1 M TS for 30 min followed by incubation for 30 min in avidin–biotin peroxidase complex (Vector Laboratories Ltd, Peterborough, UK). The peroxidase reaction product was visualised by incubation in a solution containing 0.022% of 3,3′diaminobenzidine (DAB, Aldrich) and 0.003% H_2O_2 for 6 min as described previously.[7] The reaction was stopped by rinsing the sections in 0.1 M TS for 6 min followed by 0.1 M PB for 15 min.

For detection and determination of SERT-IR fibre and its relationship with Aβ senile plaques, we used dual indirect immunofluorescence labelling. The sections were incubated for 48 h at room temperature in primary antibody cocktail containing: (i) mouse anti-β amyloid monoclonal antibody (Aβ; 1 : 2000; Covance) and (ii) rabbit anti-SERT polyclonal antibody (1 : 2500, Immunostar) simultaneously. Subsequently, Aβ plaques and SERT-IR fibres were detected in a sequential manner on the same sections by incubation with Alexa 595 goat anti-mouse and Alexa 488 goat anti-rabbit (Invitrogen, Paisley, UK) IgG, respectively. Finally, sections were rinsed with 0.1 M PB for 30 min and permanently mounted in an aqueous medium (Vectashield; Vetor Laboratories Ltd, Peterborough, UK).

Electron microscopy. Following the DAB treatment (immunohistochemistry), brain sections were rinsed and flattened in 0.1 M PB and post-fixed in 2% osmium tetroxide in 0.1 M PB for 1 h as described previously.[27,30] The sections were then washed in 0.1 M PB for 10 min followed by sequential dehydration through replacement with graded ethanol series (30, 50, 70 and 95%, 5 min each). The sections were further dehydrated using 100% ethanol (10 min), propylene oxide (2 × 15 min) and propylene oxide/EPON (1 : 1, Agar Scientific Ltd, Stanstead, UK) overnight at room temperature rotating. The propylene oxide/EPON was replaced with 100% EPON and rotated for further 2 h. The sections were then flat embedded between sheets of Aclar fluo halocarbon film (Agar Scientific Ltd).[27,30] Polymerisation was carried out by incubating at 60 °C overnight. Following polymerisation, the region of interest (CA1 subfield of the hippocampus) was selected and micro-dissected from the flat-embedded tissue and mounted on the tip of EPON blocks[27] (Figure 1), keeping the same levels and coordinates between the different animals. Diamond knife was used to cut series of ultrathin sections of these regions at a thickness of approximately 70 nm. Series of sections were collected on degreased copper mesh grids (200 mesh) and counterstained using uranyl acetate and lead citrate[47] before examining under Philips FEI Tecnai 12 BioTwin electron microscope (FEI, Eindhoven, The Netherlands). Random images of the areas of interest (blindly taken) were collected and the negatives digitalised on an Imacon Flextight 848 scanner (Imacon Inc. Hasselblad A/S, Copenhagen, Denmark), each representing a volume of 12.39 μm^3, for a total analysed CA1 volume of 396.48 μm^3 (in each animal) and 99.12 μm^3 per each CA1 layer (S. Or, pyramidal layer, S. Rad and S. Mol).

Labelling profiles and nomenclature. The labelled profiles were classified as somata, dendrites, dendritic spines, unmyelinated axons, axon terminals and glia, according to their morphological features as described previously[27,30] and defined by Peters *et al.*[48] Synapses were defined as either symmetric when having thin pre- and postsynaptic densities or asymmetric when having a thin pre- and a thick postsynaptic membrane specialisation.[27] Perforated synapses were defined as those asymmetric synapses with a notable discontinuity (> 50 nm) in the electron density of the postsynaptic junction as previously described.[27]

Numerical density. To determine the N_v of labelled profiles (# labelled profiles/μm^3), ultrastructural analysis was entirely carried out on the most superficial portions of the tissue in contact with the embedding plastic; from both vibratome section sides, to minimise artificial differences in labelling attributed to potential differences in the penetration of reagents as described previously.[27] Regions used for this analysis were chosen randomly by a single investigator without any information about the genotype or the age of the animal. The N_v of SERT-Te, SERT-Ax and synapses was determined, on serial ultrathin sections, according to the Cavalieri principle as described elsewhere.[49]

$$N_v = \sum P/[t \cdot \alpha(p)]$$

Where N_v is the numerical density, ΣP is the number of SERT-Te, SERT-Ax or synapses counted; t is the average ultrathin section thickness and $\alpha(p)$ is the corresponding surface area. All sections used for quantitative analysis were of identical anatomical level corresponding to −2.06 mm posterior to Bregma (dorsal hippocampus) in both 3xTg-AD and non-Tg control animals.

Three vibratome sections from each of the 12 animals ($n = 3$ per group) were examined for ultrastructural quantification of SERT immunolabelled profiles. The N_v of labelled profiles were determined and identified by the presence of amorphous electron-dense DAB reaction product (Figures 3–5). We selected this method over immunogold labelling, because the latter is less sensitive compared with peroxidase labelling.[50] Although gold labelling allows a more selective subcellular localisation, it has reduced tissue penetration and limited diffusion that may result in an underestimation of the relative abundance of immunoreactive profiles.[27,50] Furthermore, immunogold labelling provides less reliable quantitative 3D estimation of labelled profiles because it is primarily regarded as 2D (surface) method and is not reliably considered as quantitative for 3D labelling.[50]

The total labelled profiles numbered 592 over a corresponding total volume of 4,556.16 μm^3. Using computer-assisted imaging analysis (ImageJ 1.32j, NIH, Bethesda, MD, USA), we also analysed the area of SERT-Te in all hippocampal layers, as well as their synaptic specialisations found in labelled ($SERT^+$) terminals in both 3xTg-AD and non-Tg control animals. Composite figures, adjusted for brightness, contrast and sharpness, were generated using Adobe Photoshop CS2 (Adobe Systems Inc., San Jose, CA, USA) and Microsoft Excel 2002 (Microsoft Corporation, Reading, UK).

Statistical analysis. Results are expressed as mean ± S.E.M. Unpaired Student's *t*-test was applied to determine differences in N_v of SERT-Te, SERT-Ax and synapses between 3xTg-AD and non-Tg control animals at 3 and 18 months of age. Significance was accepted at $P \leq 0.05$. The data were analysed using GraphPad Prism 4.0 (GraphPad Software, Inc., La Jolla, CA, USA).

Conflict of Interest

The authors declare no conflict of interest.

Acknowledgements. This study was supported by Alzheimer's Research Trust Programme Grant (ART/PG2004A/1) to JJR and AV. Grant Agency of the Czech Republic (GACR 309/09/1696 and GACR 304/11/0184) to JJR and (GACR 305/08/1381, GACR 305/08/1384) to AV. The Spanish Government, Plan Nacional de I + D + I 2008-2011 and ISCIII- Subdirección General de Evaluación y Fomento de la investigación (PI10/02738) to JJR and AV and the Government of the Basque Country grant (AE-2010-1-28, AEGV10/16) to JJR. We would also like to thank BBSRC for the PhD studentship to HNN.

1. Braak E, Griffing K, Arai K, Bohl J, Bratzke H, Braak H. Neuropathology of Alzheimer's disease: what is new since A. Alzheimer? *Eur Arch Psychiatry Clin Neurosci* 1999; **249**: 14–22.
2. Selkoe DJ. Alzheimer's disease is a synaptic failure. *Science* 2002; **298**: 789–791.
3. Knight RA, Verkhratsky A. Neurodegenerative diseases: failures in brain connectivity? *Cell Death Differ* 2010; **17**: 1069–1070.
4. Birks JS, Melzer D, Beppu H. Donepezil for mild and moderate Alzheimer's disease. *Cochrane Database Syst Rev* 2000; **4**: CD001190.
5. Rupsingh R, Borrie M, Smith M, Wells JL, Bartha R. Reduced hippocampal glutamate in Alzheimer disease. *Neurobiol Aging* 2011; **32**: 802–810.
6. Mowla A, Mosavinasab M, Haghshenas H, Borhani Haghighi A. Does serotonin augmentation have any effect on cognition and activities of daily living in Alzheimer's dementia? A double-blind, placebo-controlled clinical trial. *J Clin Psychopharmacol* 2007; **27**: 484–487.
7. Noristani HN, Olabarria M, Verkhratsky A, Rodriguez JJ. Serotonin fibre sprouting and increase in serotonin transporter immunoreactivity in the CA1 area of hippocampus in a triple transgenic mouse model of Alzheimer's disease. *Eur J Neurosci* 2010; **32**: 71–79.
8. Vertes RP, Fortin WJ, Crane AM. Projections of the median raphe nucleus in the rat. *J Comp Neurol* 1999; **407**: 555–582.
9. Schmitt JA, Wingen M, Ramaekers JG, Evers EA, Riedel WJ. Serotonin and human cognitive performance. *Curr Pharm Des* 2006; **12**: 2473–2486.
10. Garcia-Alloza M, Gil-Bea FJ, Diez-Ariza M, Chen CP, Francis PT, Lasheras B *et al.* Cholinergic-serotonergic imbalance contributes to cognitive and behavioral symptoms in Alzheimer's disease. *Neuropsychologia* 2005; **43**: 442–449.

11. Liu Y, Yoo MJ, Savonenko A, Stirling W, Price DL, Borchelt DR *et al.* Amyloid pathology is associated with progressive monoaminergic neurodegeneration in a transgenic mouse model of Alzheimer's disease. *J Neurosci* 2008; **28**: 13805–13814.
12. Aucoin JS, Jiang P, Aznavour N, Tong XK, Buttini M, Descarries L *et al.* Selective cholinergic denervation, independent from oxidative stress, in a mouse model of Alzheimer's disease. *Neuroscience* 2005; **132**: 73–86.
13. Holm P, Ettrup A, Klein AB, Santini MA, El-Sayed M, Elvang AB *et al.* Plaque deposition dependent decrease in 5-HT2A serotonin receptor in AbetaPPswe/PS1dE9 amyloid overexpressing mice. *J Alzheimers Dis* 2010; **20**: 1201–1213.
14. Harkany T, Dijkstra IM, Oosterink BJ, Horvath KM, Abraham I, Keijser J *et al.* Increased amyloid precursor protein expression and serotonergic sprouting following excitotoxic lesion of the rat magnocellular nucleus basalis: neuroprotection by Ca(2+) antagonist nimodipine. *Neuroscience* 2000; **101**: 101–114.
15. Harkany T, O'Mahony S, Keijser J, Kelly JP, Konya C, Borostyankoi ZA *et al.* Beta-amyloid(1-42)-induced cholinergic lesions in rat nucleus basalis bidirectionally modulate serotonergic innervation of the basal forebrain and cerebral cortex. *Neurobiol Dis* 2001; **8**: 667–678.
16. Verdurand M, Berod A, Le Bars D, Zimmer L. Effects of amyloid-beta peptides on the serotoninergic 5-HT(1A) receptors in the rat hippocampus. *Neurobiol Aging* 2011; **32**: 103–114.
17. Zhou FC, Azmitia EC, Bledsoe S. Rapid serotonergic fiber sprouting in response to ibotenic acid lesion in the striatum and hippocampus. *Brain Res Dev Brain Res* 1995; **84**: 89–98.
18. Phinney AL, Deller T, Stalder M, Calhoun ME, Frotscher M, Sommer B *et al.* Cerebral amyloid induces aberrant axonal sprouting and ectopic terminal formation in amyloid precursor protein transgenic mice. *J Neurosci* 1999; **19**: 8552–8559.
19. Huang J, Pickel VM. Serotonin transporters (SERTs) within the rat nucleus of the solitary tract: subcellular distribution and relation to 5HT2A receptors. *J Neurocytol* 2002; **31**: 667–679.
20. Oddo S, Caccamo A, Shepherd JD, Murphy MP, Golde TE, Kayed R *et al.* Triple-transgenic model of Alzheimer's disease with plaques and tangles: intracellular Abeta and synaptic dysfunction. *Neuron* 2003; **39**: 409–421.
21. DeKosky ST, Scheff SW. Synapse loss in frontal cortex biopsies in Alzheimer's disease: correlation with cognitive severity. *Ann Neurol* 1990; **27**: 457–464.
22. Scheff SW, Price DA, Schmitt FA, Mufson EJ. Hippocampal synaptic loss in early Alzheimer's disease and mild cognitive impairment. *Neurobiol Aging* 2006; **27**: 1372–1384.
23. King DL, Arendash GW. Maintained synaptophysin immunoreactivity in Tg2576 transgenic mice during aging: correlations with cognitive impairment. *Brain Res* 2002; **926**: 58–68.
24. Buttini M, Yu GQ, Shockley K, Huang Y, Jones B, Masliah E *et al.* Modulation of Alzheimer-like synaptic and cholinergic deficits in transgenic mice by human apolipoprotein E depends on isoform, aging, and overexpression of amyloid beta peptides but not on plaque formation. *J Neurosci* 2002; **22**: 10539–10548.
25. Yao PJ, Bushlin I, Furukawa K. Preserved synaptic vesicle recycling in hippocampal neurons in a mouse Alzheimer's disease model. *Biochem Biophys Res Commun* 2005; **330**: 34–38.
26. Bertoni-Freddari C, Sensi SL, Giorgetti B, Balietti M, Di Stefano G, Canzoniero LM *et al.* Decreased presence of perforated synapses in a triple-transgenic mouse model of Alzheimer's disease. *Rejuvenation Res* 2008; **11**: 309–313.
27. Rodriguez JJ, Doherty MD, Pickel VM. N-methyl-D-aspartate (NMDA) receptors in the ventral tegmental area: subcellular distribution and colocalization with 5-hydroxytryptamine(2A) receptors. *J Neurosci Res* 2000; **60**: 202–211.
28. Wirths O, Multhaup G, Bayer TA. A modified beta-amyloid hypothesis: intraneuronal accumulation of the beta-amyloid peptide–the first step of a fatal cascade. *J Neurochem* 2004; **91**: 513–520.
29. Miguel-Hidalgo JJ, Alvarez XA, Cacabelos R, Quack G. Neuroprotection by memantine against neurodegeneration induced by beta-amyloid(1-40). *Brain Res* 2002; **958**: 210–221.
30. Peddie CJ, Davies HA, Colyer FM, Stewart MG, Rodriguez JJ. Dendritic colocalisation of serotonin1B receptors and the glutamate NMDA receptor subunit NR1 within the hippocampal dentate gyrus: an ultrastructural study. *J Chem Neuroanat* 2008; **36**: 17–26.
31. Ogren SO, Eriksson TM, Elvander-Tottie E, D'Addario C, Ekstrom JC, Svenningsson P *et al.* The role of 5-HT(1A) receptors in learning and memory. *Behav Brain Res* 2008; **195**: 54–77.
32. Truchot L, Costes SN, Zimmer L, Laurent B, Le Bars D, Thomas-Anterion C *et al.* Up-regulation of hippocampal serotonin metabolism in mild cognitive impairment. *Neurology* 2007; **69**: 1012–1017.
33. Geinisman Y, de Toledo-Morrell L, Morrell F. Loss of perforated synapses in the dentate gyrus: morphological substrate of memory deficit in aged rats. *Proc Natl Acad Sci USA* 1986; **83**: 3027–3031.
34. Nicholson DA, Yoshida R, Berry RW, Gallagher M, Geinisman Y. Reduction in size of perforated postsynaptic densities in hippocampal axospinous synapses and age-related spatial learning impairments. *J Neurosci* 2004; **24**: 7648–7653.
35. Geinisman Y, Ganeshina O, Yoshida R, Berry RW, Disterhoft JF, Gallagher M. Aging, spatial learning, and total synapse number in the rat CA1 stratum radiatum. *Neurobiol Aging* 2004; **25**: 407–416.
36. Delatour B, Guegan M, Volk A, Dhenain M. *In vivo* MRI and histological evaluation of brain atrophy in APP/PS1 transgenic mice. *Neurobiol Aging* 2006; **27**: 835–847.
37. Schmitz C, Rutten BP, Pielen A, Schafer S, Wirths O, Tremp G *et al.* Hippocampal neuron loss exceeds amyloid plaque load in a transgenic mouse model of Alzheimer's disease. *Am J Pathol* 2004; **164**: 1495–1502.
38. Valla J, Schneider L, Reiman EM. Age- and transgene-related changes in regional cerebral metabolism in PSAPP mice. *Brain Res* 2006; **1116**: 194–200.
39. Oberg J, Spenger C, Wang FH, Andersson A, Westman E, Skoglund P *et al.* Age related changes in brain metabolites observed by 1H MRS in APP/PS1 mice. *Neurobiol Aging* 2008; **29**: 1423–1433.
40. Maheswaran S, Barjat H, Rueckert D, Bate ST, Howlett DR, Tilling L *et al.* Longitudinal regional brain volume changes quantified in normal aging and Alzheimer's APP x PS1 mice using MRI. *Brain Res* 2009; **1270**: 19–32.
41. Coggeshall RE, Lekan HA. Methods for determining numbers of cells and synapses: a case for more uniform standards of review. *J Comp Neurol* 1996; **364**: 6–15.
42. Stewart MG, Medvedev NI, Popov VI, Schoepfer R, Davies HA, Murphy K *et al.* Chemically induced long-term potentiation increases the number of perforated and complex postsynaptic densities but does not alter dendritic spine volume in CA1 of adult mouse hippocampal slices. *Eur J Neurosci* 2005; **21**: 3368–3378.
43. Yoshiyama Y, Higuchi M, Zhang B, Huang SM, Iwata N, Saido TC *et al.* Synapse loss and microglial activation precede tangles in a P301S tauopathy mouse model. *Neuron* 2007; **53**: 337–351.
44. Nelson RL, Guo Z, Halagappa VM, Pearson M, Gray AJ, Matsuoka Y *et al.* Prophylactic treatment with paroxetine ameliorates behavioral deficits and retards the development of amyloid and tau pathologies in 3xTgAD mice. *Exp Neurol* 2007; **205**: 166–176.
45. Paxinos G, Franklin KBJ. *The Mouse Brain in Stereotaxic Coordinates* 2nd edn Elesvier Academic Press: San Diego, 2004.
46. Albright MJ, Weston MC, Inan M, Rosenmund C, Crair MC. Increased thalamocortical synaptic response and decreased layer IV innervation in GAP-43 knockout mice. *J Neurophysiol* 2007; **98**: 1610–1625.
47. Reynolds ES. The use of lead citrate at high pH as an electron-opaque stain in electron microscopy. *J Cell Biol* 1963; **17**: 208–212.
48. Peters A, Palay SL, Webster HD. *The Fine Structure of the Nervous System*. Oxford UP: New York, 1991.
49. Tang Y, Nyengaard JR, De Groot DM, Gundersen HJ. Total regional and global number of synapses in the human brain neocortex. *Synapse* 2001; **41**: 258–273.
50. Cortese K, Diaspro A, Tacchetti C. Advanced correlative light/electron microscopy: current methods and new developments using Tokuyasu cryosections. *J Histochem Cytochem* 2009; **57**: 1103–1112.

Supplementary Information accompanies the paper on Cell Death and Disease website (http://www.nature.com/cddis)